Journal of Power Sources 196 (2011) 488–494

Contents lists available at ScienceDirect

Journal of Power Sources

journal homepage: www.elsevier.com/locate/jpowsour

Cation-exchange induced high power electrochemical properties of core–shell $Ni(OH)_2$@CoOOH

Weihua Chen[a,b], Yifu Yang[a,*], Huixia Shao[a]

[a] College of Chemistry and Molecular Science, Wuhan University, 430072 Wuhan, PR China
[b] Department of Chemistry, Zhengzhou University, 450001 Zhengzhou, PR China

ARTICLE INFO

Article history:
Received 19 April 2010
Received in revised form 30 June 2010
Accepted 8 July 2010
Available online 15 July 2010

Keywords:
Cation-exchange
Core–shell
Batteries
Nickel hydroxide
Cobalt oxide hydroxide

ABSTRACT

New applications such as hybrid electric vehicles and power backup require rechargeable batteries to combine high energy density with high charge and discharge rate capability. In this study, the core–shell $Ni(OH)_2$@CoOOH composite is constructed via a simple cation-exchange route at moderate conditions. X-ray diffraction (XRD), X-ray photoelectron spectroscopy (XPS), scanning electron microscopy (SEM) with energy dispersive X-ray (EDX), and inductively coupled plasma (ICP) are used to characterize the resulting $Ni(OH)_2$@CoOOH composites. The $Ni(OH)_2$@CoOOH electrode exhibits high power, higher capacity and longer life cycle when it is chosen as an positive electrode material for rechargeable alkaline MH-Ni battery. The enhanced electrochemical performance is attributed to the seamless combination of the CoOOH shell and the $Ni(OH)_2$ core, avoiding the contact resistance between them at a large current density. It is believed that our methodology provides a simple and environment friendly route to a variety of core–shell materials with different composition and novel function.

1. Introduction

Nickel hydroxide particles with controlled structures have long been of great interest due to its significant applications in advanced nickel-based batteries [1–3], catalysts [4–6], magnetics [7,8] and ionic exchangers [9–11]. Recently, great efforts have been focused on enhancing the high power performance of it for suitable use in hybrid electric vehicles (HEVs) and electric vehicles (EVs) to overcome the shortage of energy sources and the pollution of our environment that have become more and more important [12,13]. It follows that increasing the power capabilities of this material is essential and important for raising the power performance of such batteries. However, the poor electric conductivity of $Ni(OH)_2$ (a p-type semiconductor) is the main factor that blocks the performance of it at high-rate charge and discharge [14].

Core–shell macro/nano-structures exhibit unusual catalytic, electronic, magnetic and electrochemical properties owing to its special structure [15–18]. This structure has been successfully introduced into electrochemistry system to tuning the electrochemical properties. However, only examples of surface-modified nickel hydroxide currently exist to improve the conductivity characteristics of this electrode [19–22] although significant advances have been made in developing synthetic methods to prepare nickel hydroxide particles. In addition, the regularly used coating methods including precipitation [23] and plating [19] are either difficult to be controlled or complicated and environment unfriendly. More importantly, the coating layer cannot adhere to the surface of spherical $Ni(OH)_2$ closely enough that the conductivity and cycle life of the electrode cannot be guaranteed. Therefore, it is imperative to develop alternative effective routes for the purpose of overcoming the drawbacks of the above mentioned surface-modified spherical $Ni(OH)_2$ itself and the preparation method.

Cation-exchange provides a facile method to make a chemical transformation from one solid to another via insertion and exchange of central metal atoms [24]. This method attracts intense interest recently. A range of nanocrystals of varying composition, size and shape have been achieved successfully by this effective and powerful method [24–29]. Herein, we explore to modify the surface of spherical $Ni(OH)_2$ via the exchange of nickel ions by cobalt ones to give rise to a core–shell $Ni(OH)_2$@CoOOH to improve its electrochemical properties. To the best of our knowledge, no work on cation-exchange route for modifying commercial spherical $Ni(OH)_2$ resulting core–shell structured $Ni(OH)_2$@CoOOH has been reported.

2. Experiment

2.1. Materials

All chemicals except commercial β-type spherical $Ni(OH)_2$ powder (named as A_0) used in our experiments were all of analytical

* Corresponding author. Tel.: +86 18627010125; fax: +86 27 68754067.
E-mail addresses: whucwh@hotmail.com (W. Chen), yang-y-f1@vip.sina.com (Y. Yang), shao_hx@sina.com (H. Shao).

0378-7753/$ – see front matter © 2010 Elsevier B.V. All rights reserved.
doi:10.1016/j.jpowsour.2010.07.026

Table 1
EDX and ICP results of starting commercial spherical $Ni(OH)_2$(A_0) and cation-exchange induced core–shell $Ni(OH)_2$@CoOOH product (A_1), respectively.

Sample	EDS (at.)	ICP (wt.%)		ICP (at.)
	Ni/Co	Ni	Co	Ni/Co
A_0	38.2	58.72	1.41	41.8
A_1	13.22	56.50	3.32	17.1

grade, purchased from Shanghai Chemicals Co. Ltd. (China), and used without further purification. The water used for solution preparation is deionized water (resistivity ≥18 MΩ, water purification system). The commercial β-type spherical nickel hydroxide powder was purchased from Kelong Co. Ltd. (China) used as precursor.

2.2. Sample preparation

The core–shell $Ni(OH)_2$@CoOOH (A_1) was prepared as follows: firstly, 2.25 mmol $Co(NO_3)_2{\cdot}6H_2O$ was dissolved in 50 mL deionized water, and then, the commercial β-type spherical $Ni(OH)_2$ powder (10 mmol) was launched into the solution followed by dropwise adding a 30% H_2O_2 solution (8 mL) at 90 °C. After the mixed solution was continuously stirred for 2 h, it was cooled naturally to room temperature and was centrifugated. The solid product was subsequently washed for several times with deionized water and ethanol, and then dried in air at 65 °C for 12 h. By operating the whole process, ca. 1 g solid powder of sample A_1 was obtained at a time. The metal compositions of as-synthesized A_1 and the starting material A_0 were listed in Table 1.

When the reaction conditions of the aforementioned procedure, such as nickel source, reaction temperature or ratio of reactants, were changed, a series of products could be obtained. The specific conditions were listed in Table 2. The corresponding samples were named and also listed in Table 2.

2.3. Physical characterization

The lattice structures of the reactant and resulted spherical core–shell $Ni(OH)_2$@CoOOH particles were examined by taking powder X-ray diffraction (XRD) patterns for the dried samples with a XRD-6000 (Cu Kα radiation, Shimadzu, Japan). Scanning electron micrographs (SEM) of the spherical particles were acquired using a JSM-6390/LV (JEOL, Japan) scanning electron microscope. The elemental composition of as-synthesized $Ni(OH)_2$@CoOOH was obtained from energy dispersive X-ray analysis (EDX) and inductively coupled plasma (ICP) measurements (Thermo., USA), respectively. The oxidation states of Ni and Co cations in the product phase were determined from X-ray photoelectron spectroscopy (XPS) (XSAM800, Kratos Ltd., UK).

2.4. Electrochemical characterization

Galvanostatic charge–discharge of sample A_1 was measured as follows: powder of sample A_1 was mixed with graphite powder and PTFE suspension (60% suspension) in weight ratios of 87:10:3 with a mixed solvent of water and organic one. The thoroughly mixed paste was sandwiched into two nickel foams. They were pressed at pressure of 120 kg cm^{-2} at room temperature and dried at 70 °C for several hours. Galvanostatic charge–discharge tests were conducted with a battery performance-testing instrument (Land Test Equipment, CT2001A), with two pieces of negative electrodes made from commercial AB_5 hydrogen storage alloys as counter electrodes on either side of the working electrode, and a 6 M KOH solution as the electrolyte. All capacities are normalized to the nickel content of the active materials (estimated by ICP). All the tests were conducted at 25 ± 2 °C.

In addition, a 6 Ah prismatic power battery was assembled employed the positive electrode which consists of powder of sample A_1 and PTFE suspension (60% suspension) in weight ratios of 98:2. The negative electrode made from commercial AB_5 hydrogen storage alloys. The electrolyte is 6 M KOH solution. Galvanostatic charge–discharge tests were conducted with a battery performance-testing instrument (Arbin BT-2000). The cell resistance was measured by the dc-pulse method. All the tests were conducted at 25 ± 2 °C.

3. Results and discussions

Cation-exchange treatment of commercial spherical $Ni(OH)_2$ (A_0) by cobalt ions in the presence of H_2O_2 was used to modify the surface of nickel hydroxide particles (Scheme 1). After the cation-exchange treatment, the beige-colored product (A_1) indicating the formation of CoOOH could be obtained as shown in their photos in the inserts of Fig. 1a and d, different from the light green color of A_0. Here, the H_2O_2 behaves as the oxidant to form CoOOH. The exchange of Ni^{2+} by Co^{2+} proceeds difficultly in the surface layer of nickel hydroxide particles because of the nature of these two kinds of cations that ion radii of Co^{2+} (74 pm) is much similar with that of Ni^{2+} (72 pm) as well as their similar Ksp values [29]. Fortunately, the obtained $Co(OH)_2$ is prone to be oxidized to CoOOH in aqueous solution at the presence of oxidants which benefits the cation-exchange process.

The central metal compositions of A_0 and A_1 were analyzed by ICP-OES and EDX shown in Table 1. The molar ratio of Ni/Co (i.e. 38.2) of A_1 coming from EDX result (the inset of Fig. 1c) is quite close to ICP result (41.8) because of the well-proportioned distribution of cobalt ions in it. Whereas the EDX result (Ni/Co = 13.22) of cation-exchange induced A_1 (the inset of Fig. 1f) is obviously smaller than ICP result (Ni/Co = 17.1) of it. This means that the content of cobalt in the surface layer of the spherical particles, which is in the depth extension of EDX, is much higher than the average content of the whole particle bodies in accordance with the color

Table 2
Preparation conditions and relative element content for different samples.

Sample	Cobalt source	Molar ratio of reaction solution (Ni/Co)	30% H_2O_2 (mL)	Temperature (°C)	Reaction time (h)	ICP (wt.%) (Co)
A_0	–	–	–	–	–	1.41
B	Sulphates	9:2	8	90	2	3.56
C	Chlorides	9:2	8	90	2	3.27
D	Ethanoates	9:2	8	90	2	1.99
A_1	Nitrates	9:2	8	90	2	3.32
A_2	Nitrates	9:2	8	70	2	2.76
A_3	Nitrates	9:2	8	50	2	2.14
A_4	Nitrates	9: 0.5	2	90	2	1.99
A_5	Nitrates	9:1	4	90	2	2.61
A_6	Nitrates	9:3	12	90	2	4.16

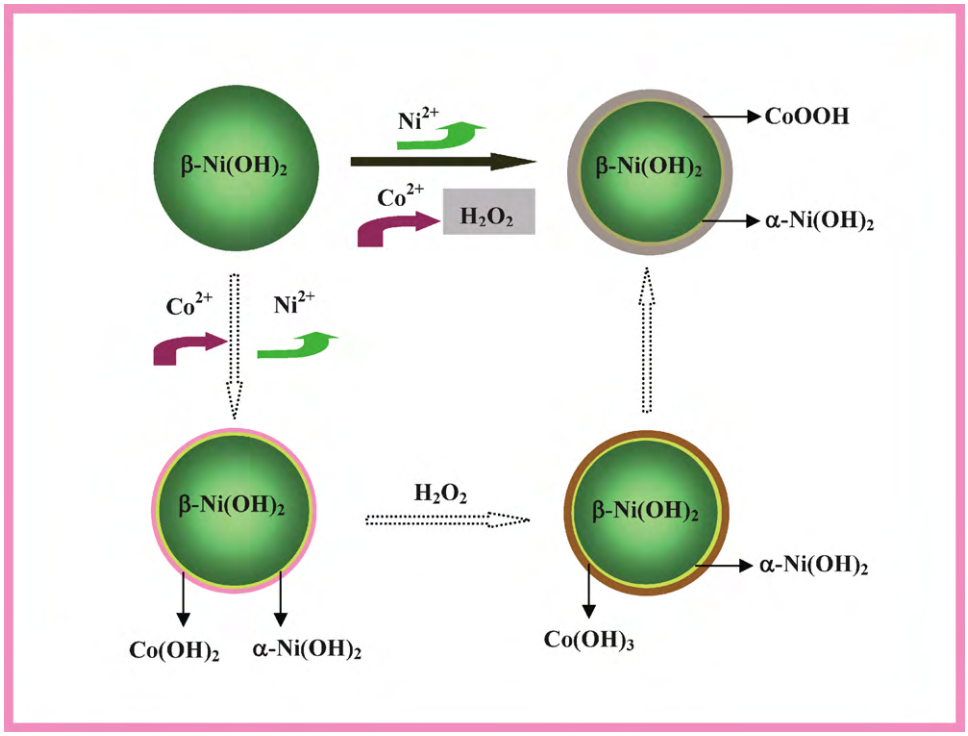

Scheme 1. Synthetic scheme and proposed structure of core–shell $Ni(OH)_2$@CoOOH.

change of the two kinds of material. This indicates that exchange of nickel with cobalt mainly occurs in the surface layer of the spherical particles suggesting a core–shell structure of A_1. Thanks to the characteristics of cation-exchange method, there isn't ordinary interface between the shell and the $Ni(OH)_2$ core but very likely to be a transitional phase which was attributed to the partial cation exchange. The structure is like that of watermelon. Therefore, the combination between the shell and the $Ni(OH)_2$ core should be exclusively firm.

The SEM images of initial commercial substance A_0 (Fig. 1a) and cation-exchange induced product A_1 (Fig. 1d) at low resolution indicate that the size distributions of these two kinds of particle do not exhibit obvious difference, approximately in the range of 10–25 μm. Their SEM images of single particles (Fig. 1b and e) show that these two kinds of particle have extremely similar smooth and compact surfaces implying that the cation-exchange treatment does not affect the surface feature of particles. Furthermore, high resolution images of them (Fig. 1c and f) display the

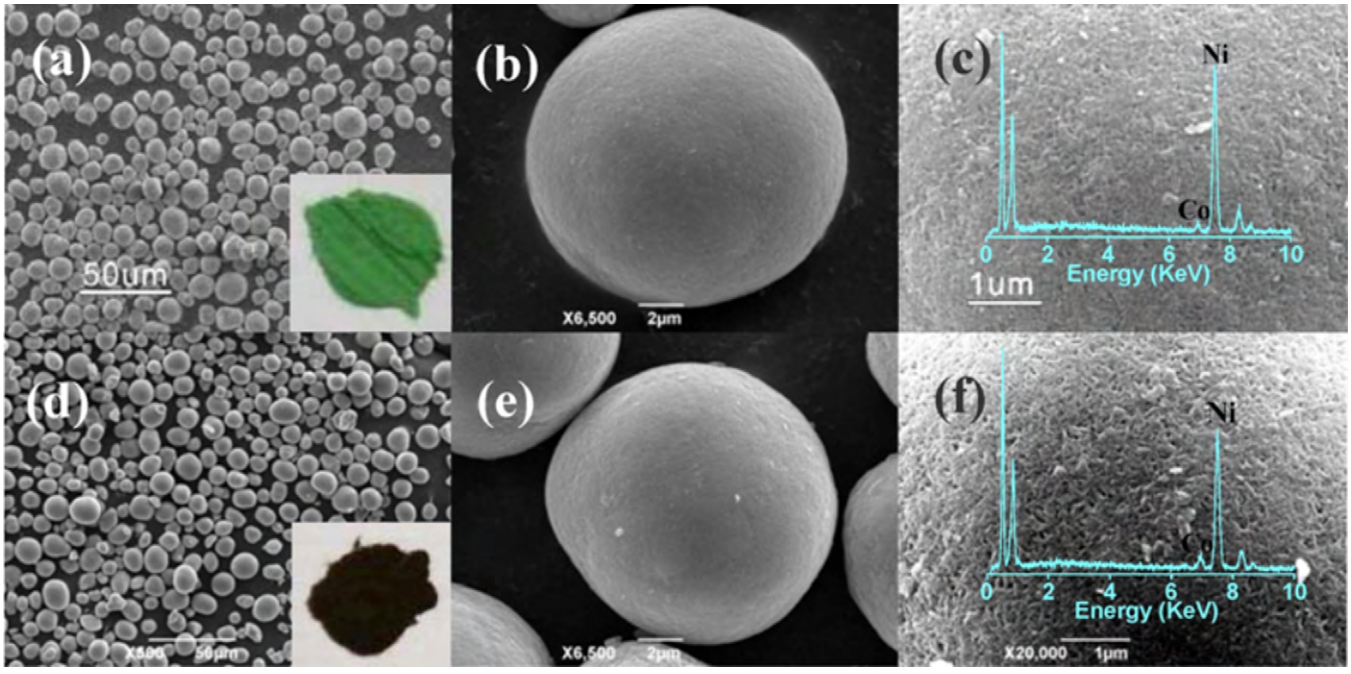

Fig. 1. Typical SEM images of starting spherical nickel hydroxide A_0 (a–c) and cation-exchange induced core–shell $Ni(OH)_2$@CoOOH product A_1 (d–f); the insets of (a and d) are the photos A_0 and A_1; The insets of (c and f) are their EDX spectrum.

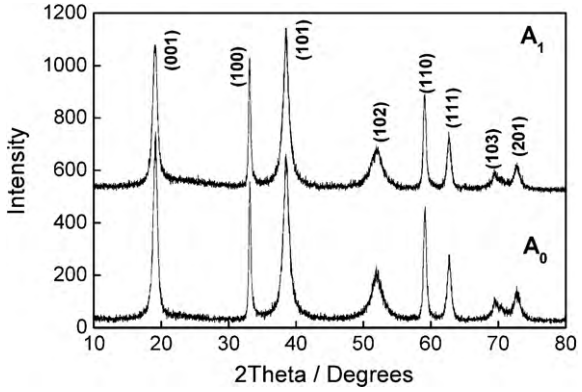

Fig. 2. XRD patterns of starting spherical nickel hydroxide A_0 and cation-exchange induced core–shell $Ni(OH)_2$@CoOOH product A_1.

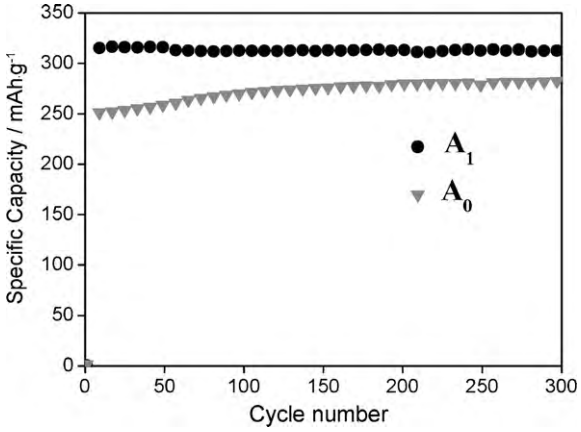

Fig. 4. Variations of the capacity of A_0 and A_1 *vs.* cycle numbers of the cells.

surface morphology of them, from which it can be seen that both are constructed by crossed shuttles. All these results manifest the effectiveness of cation-exchange process in preserving the shape and morphology of the precursor owing to the cation-exchange reaction taking place in situ.

XRD patterns of A_0 and A_1 were displayed in Fig. 2 showing a closely similar diffraction peaks. This is reasonable because the too thin layer of CoOOH was produced in the surface layer of the spherical particles of A_0 so that XRD cannot give clear information about it. The XRD pattern of A_0 corresponds to the well-crystalline β-$Ni(OH)_2$ phase (JCPDS no. 14-0117) displaying a hexagonal lattice (a = 3.12 Å and c = 4.62 Å) [30]. The peaks at d = 4.64, 2.70, 2.33, 1.76, 1.56, 1.48, 1.35 and 1.30 Å correspond to (0 0 1), (1 0 0), (1 0 1), (1 0 2), (1 1 0), (1 1 1), (1 0 3) and (2 0 1) reflections, respectively.

To further study the surface chemical states, Co2p and Ni2p core level spectra of the as-synthesized A_1 sample were recorded as shown in Fig. 3. The Co2p3/2 signal shows a well-resolved peak at 780.3 eV of BE assigned to the Co(III) species(i.e. CoOOH) which fits well with the beige color of A_1. And the absence of any additional shake-up contributes to the higher binding energy of the main 2p3/2 line, indicative of the absence of Co(II) oxidation state. The characteristic peak (binding energy) of Ni2p locates at 855.60 eV, corresponding to the Ni(II) oxidation state [14,31]. It is undoubted that the shell of A_1 should be CoOOH as the result of cation-exchange treatment.

Charge–discharge cycle performance of electrode A_1 and A_0 in 500 cycles at the discharge rate of 2C after the same activation program is shown in Fig. 4. Electrode A_1 presents not only high discharge capacity as high as 300 mAh g^{-1} but also outstanding cycling durability in 500 cycles. In the case of electrode A_0, the discharge capacity is ca. 250–270 mAh g^{-1} in the first hundred cycles though maintaining good cycling durability as that of electrode A_1. Obviously, electrode A_1 is easily to be activated as compared to electrode A_0. Fig. 5 shows the charge–discharge curves of A_1 and A_0 electrodes at the 500th cycle. The discharge curve of electrode A_1 displays a higher discharging potential, a longer plateau and a lower charging potential than those of the A_0 electrode indicating the better conductivity and higher material utility of A_1. Furthermore, the highest discharge capacity of electrode A_1 reaches 310 mAh g^{-1} at the discharge rate of 2C, which is much higher than that of electrode A_0 (284 mAh g^{-1}). That is also higher than the theoretical capacity of β-phase nickel hydroxide (289 mAh g^{-1}) illustrating the number of exchangeable electron per nickel atom (NEE) is more than one. This could be explained by the structure of A_1 in which a transitional phase of Ni-Co hydroxide between CoOOH layer and the core of $Ni(OH)_2$ (Scheme 1, the yellow part of the resulting $Ni(OH)_2$@CoOOH) is thought as α-phase nickel hydroxide [32–34].

For investigating high-rate discharge performance of as-synthesized core–shell $Ni(OH)_2$@CoOOH, a prismatic power battery (B_1) was assembled with real capacity of 5.7 Ah without any additive for increasing the conductivity of positive electrode. For compare, another prismatic power battery (B_0) using A_0 as positive material with CoO as additive was assembled, which has a capacity of 6.1 Ah. The amount of the added CoO is equal to that of the CoOOH in the surface layer of A_1. Fig. 6 displays the discharge efficiency (η) of these two batteries at different discharge rates. The

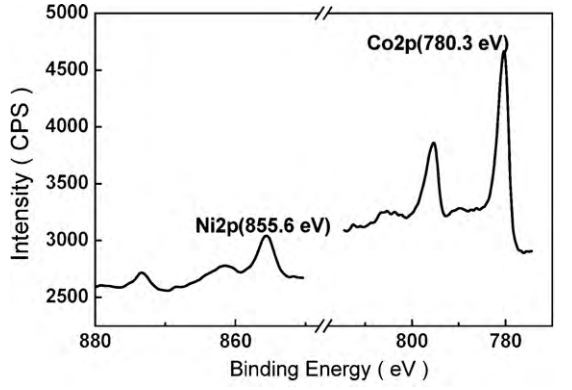

Fig. 3. Co2p and Ni2p core level spectra of the cation-exchange induced core–shell $Ni(OH)_2$@CoOOH product A_1.

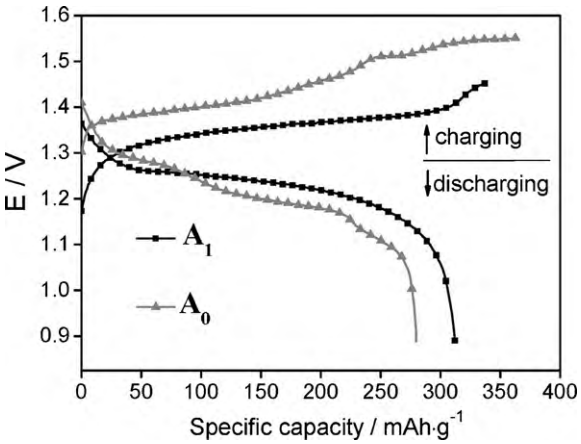

Fig. 5. Galvanostatic charge–discharge curves of A_0 and A_1.

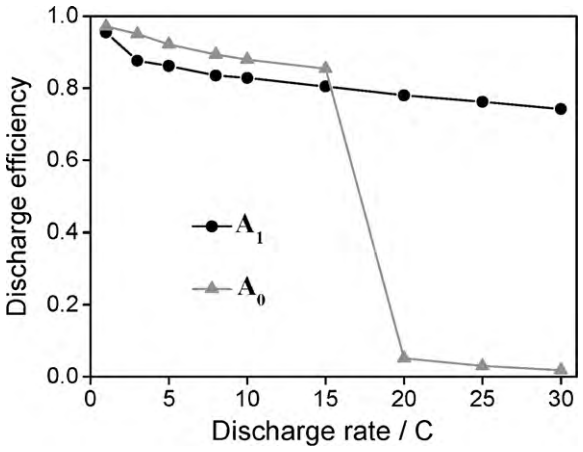

Fig. 6. Discharge efficiencies of 6 Ah prismatic type MH-Ni batteries at different discharge rates. The positive active materials are A_1 and A_0, respectively.

discharge efficiency here is defined as follows:

$$\eta_n = \frac{C_n}{C_n + C'_n} \times 100\% \quad (1)$$

where η_n is the discharge efficiency of battery at the discharge rate of nC; C_n is the available discharge capacity at the rate of nC; C'_n represents the available residual capacity obtained at $1C$ after nC rate discharge. When the discharge rate $\leq$15C, B_1 does not show merits as compared to B_0 in discharge efficiencies. However, the discharge efficiency of B_0 falls sharply as the discharge rate >15C and it just keeps 1.86% at the rate of 30C. Surprisingly, that of B_1 also maintains 74.19% when the discharge rate reaches 30C. At the same time, B_1 behaves higher discharge potential than that of B_0 at same discharge rates as shown in Fig. 7. Moreover, the resistance of B_1 is lower than that of B_0 by 1.4 mΩ, about 40% of that of B_1. It is believed that the excellent power properties of B_1 should benefit from the shell of CoOOH in the surface layer of spherical nickel hydroxide particles which enhanced intensely the conductivity of the materials, on the other hand, the firm combination between shell of CoOOH and the core of $Ni(OH)_2$ can avoid the contact resistance between the shell of CoOOH and the core of $Ni(OH)_2$.

To extend this work further, reaction conditions such as nickel source, reaction temperature, and ratio of reactants were changed. First, samples A_1, B, C, and D were obtained when cobalt nitrate, cobalt sulphate, cobalt chloride, and cobalt ethanoate were used as reactants, respectively, to synthesize the core–shell $Ni(OH)_2$@CoOOH. The colors of cation-exchanged induced samples A_1, B, C, and D are all different from the light green color of the starting material A_0, implying that the exchange cobalt with nickel is located at the surface of Ni $(OH)_2$ particles. However, the colors of samples A_1, B, and C are clearly deeper than that of sample D (Fig. 8a). In addition, ICP results reveal little difference in the cobalt content of samples A_1, B, and C, while that of sample D is obviously lower than the others (Table 2). Thus, the deeper color of the sample suggests a higher cobalt content. The probable reason for the lower cobalt content in sample D is that cobalt ethanoate has little dissociation constant, meaning there is a lower concentration of cobalt ion.

Next, when the reaction temperature was set at 90, 70, and 50 °C, respectively, samples A_1, A_2, and A_3 were obtained. As shown in Fig. 8b, cobalt content increases from A_3 to A_1, which is consistent with the ICP results (Table 2).

Lastly, when the Ni/Co ratios of reactants were set at 9:0.5, 9:1, 9:2, and 9:3, the obtained samples A_4, A_5, A_1, and A_6 had increasing content in sequence, respectively (Table 2). This result matches well with the photographs presented (Fig. 8c).

From the aforementioned understanding of the cation-exchange reaction, the mechanism of this process was considered to include three steps, as shown in Eqs. (2)–(4). As a result, the overall reaction could be summarized as Eq. (5). The reaction process was displayed in Scheme 1, in which the overall one was connected by solid arrow and the detailed process was linked by dotted arrow. In the reaction process, steps 3 and 4 are fast because of the nature of $Co(OH)_2$ and $Co(OH)_3$. Hence, step 2 is the rate-determining step, that is to say, the cation-exchange process determines the thickness of the shell. When the concentration of cobalt ion in solution was raised, the reaction deepens and the shell can become thicker. This speculation was supported by the aforementioned results. Moreover, the increase of reaction temperature could also accelerate the reaction according to Eq. (2). This was also confirmed by the result of the experiments. In addition, step 2 can lead to the products $Co(OH)_2$ and $Ni_{1-x}Co_x(OH)_2$. The product $Co(OH)_2$ could transfer to CoOOH on the surface of sample particles. However, product $Ni_{1-x}Co_x(OH)_2$ inside just keeps its structure because the produced CoOOH blocks further cation-exchange process such that $Ni_{1-x}Co_x(OH)_2$ cannot change into $Co(OH)_2$. This can be a reasonable explanation for the existence of the transition region within the structure of α-$Ni(OH)_2$.

$$Co^{2+} + Ni(OH)_2 \underset{\Delta}{\rightarrow} Ni^{2+} + Co(OH)_2 \quad (2)$$

$$2Co(OH)_2 + H_2O_2 \underset{\Delta}{\rightarrow} 2Co(OH)_3 \quad (3)$$

$$Co(OH)_3 \underset{\Delta}{\rightarrow} CoOOH + H_2O \quad (4)$$

$$2Co^{2+} + 2Ni(OH)_2 + H_2O_2 \underset{\Delta}{\rightarrow} 2Ni^{2+} + 2CoOOH + H_2O \quad (5)$$

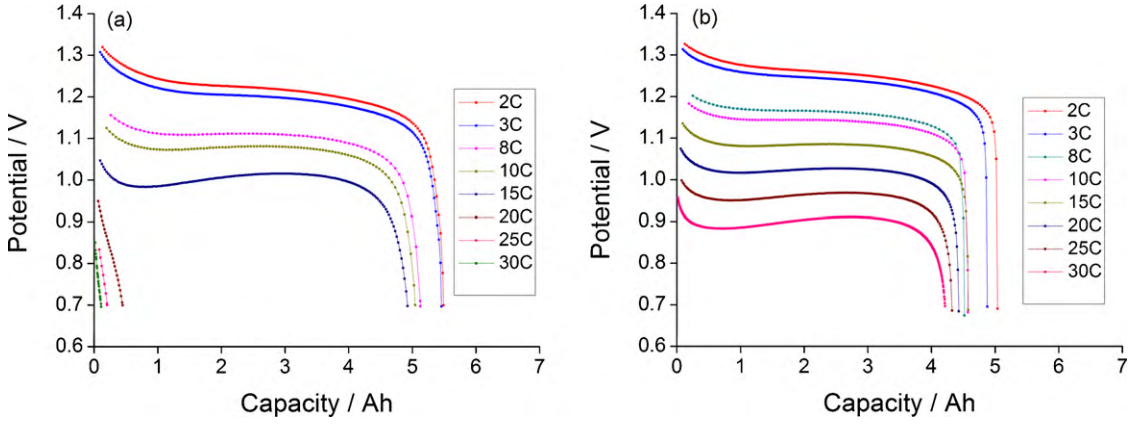

Fig. 7. Discharge curves of 6 Ah prismatic type MH-Ni batteries at different discharge currents: (a) the positive is composed of starting spherical nickel hydroxide with the addition of CoO; (b) the positive is composed of cation-exchange induced core–shell $Ni(OH)_2$@CoOOH and no any CoO was added for raising the conductivity.

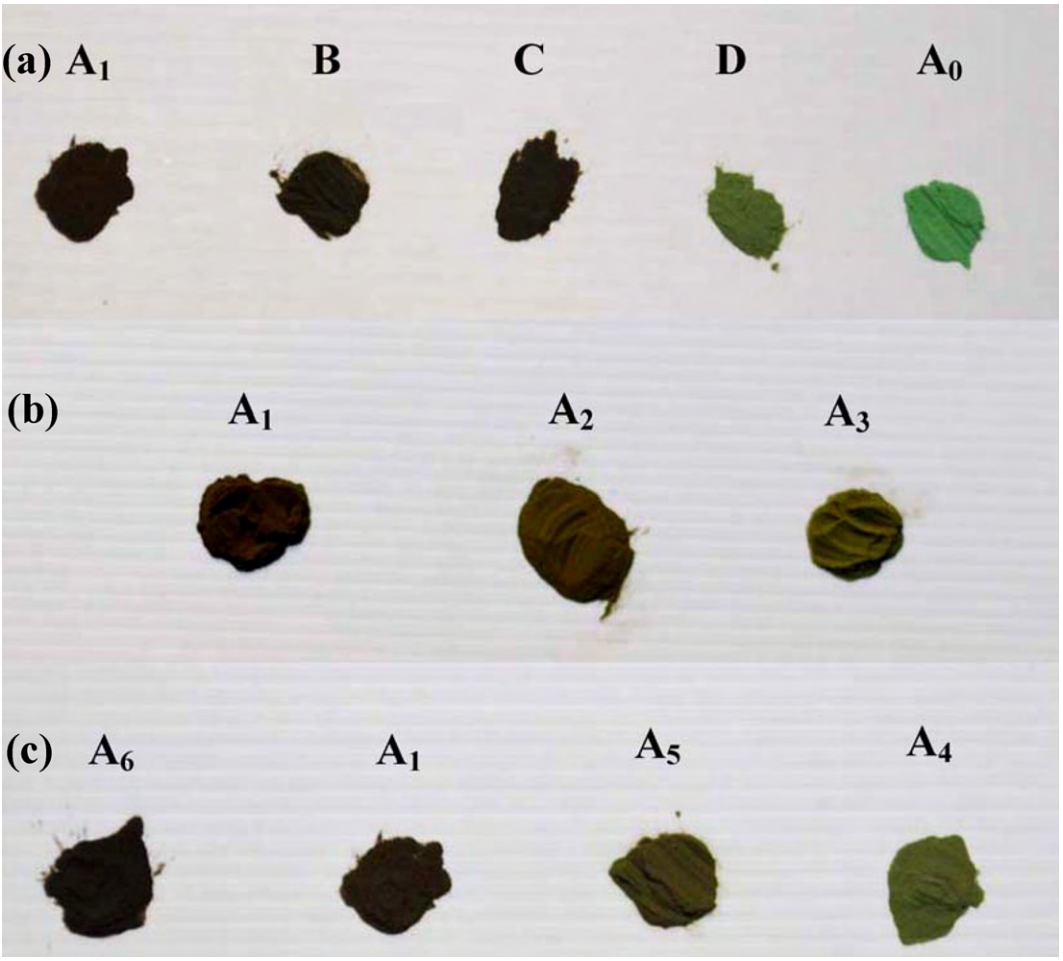

Fig. 8. (a) The photos of cation-exchange induced core–shell $Ni(OH)_2$@CoOOH samples A_1, B, C, D prepared with cobalt nitrate, cobalt sulphate, cobalt chloride, and cobalt ethanoate as nickel sources, respectively, and starting spherical nickel hydroxide A_0; (b) the photos of cation-exchange induced core–shell $Ni(OH)_2$@CoOOH samples A_1, A_2, A_3 synthesized at 90, 70, and 50 °C, respectively; (c) The photos of cation-exchange induced core–shell $Ni(OH)_2$@CoOOH samples A_6, A_1, A_5, A_4 prepared when molar ratios of Ni/Co in solutions are 9:3, 9:2, 9:1, and 9:0.5, respectively.

4. Conclusions

In conclusion, we have explored a new route to prepare core–shell $Ni(OH)_2$@CoOOH on a large scale and the reaction mechanism of the process was investigated thoroughly. The prepared core–shell structured $Ni(OH)_2$@CoOOH exhibits unusual firm combination between the shell CoOOH and the core of $Ni(OH)_2$. The conductivity of starting $Ni(OH)_2$ is improved highly by the modification of CoOOH in the surface of $Ni(OH)_2$. Furthermore, the as-synthesized $Ni(OH)_2$@CoOOH performs not only higher utilization but also outstanding cycling durability by remaining 97.7% of the highest discharge capacity after 500 cycling as positive material. Moreover, the power performance of material is improved markedly, especially when discharge rate reaches 30C which meets the demanding of HEVs or EVs perfectly, implying great potential in industrial application. In addition, this research open a wide way to improve the main properties of chemical, physical and energy materials by modifying their surface through cation-exchange route without change their original structure.

Acknowledgement

This work was supported by the 863 National Research and Development Project Foundation of China (2006AA11A152).

References

[1] J. McBreen, in: R.E. White, J.O.M. Bockris, B.E. Conway (Eds.), Modern Aspects of Electrochemistry, vol. 21, Plenum Press, New York, 1990, p. 29.
[2] F.S. Cai, G.Y. Zhang, J. Chen, X.L. Gou, H.K. Liu, S.X. Dou, Angew. Chem. Int. Ed. 43 (2004) 4212.
[3] M.H. Cao, X.Y. He, J. Chen, C.W. Hu, Cryst. Growth Des. 7 (2007) 170.
[4] T. He, D.R. Chen, X.L. Jiao, Y.L. Wang, Y.Z. Duan, Chem. Mater. 17 (2005) 4023.
[5] L.X. Yang, Y.J. Zhu, L. Li, L. Zhang, H. Tong, W.W. Wang, G.F. Cheng, J.F. Zhu, Eur. J. Inorg. Chem. 23 (2006) 4787.
[6] C. Coudun, E. Amblard, J. Guihaumé, J.-F. Hochepied, Catal. Today 124 (2007) 49.
[7] M. Kurmoo, Chem. Mater. 11 (1999) 3370.
[8] J. Pérez-Ramírez, A. Ribera, F. Kapteijn, E. Coronadob, C.J. Gómez-García, J. Mater. Chem. 12 (2002) 2370.
[9] M. Taibi, S. Ammar, N. Jouini, F. Fiévet, P. Molinié, M. Drillon, J. Mater. Chem. 12 (2002) 3238.
[10] Z.P. Liu, R.Z. Ma, M. Osada, N. Iyi, Y. Ebina, K. Takada, T. Sasaki, J. Am. Chem. Soc. 128 (2006) 4872.
[11] R.Z. Ma, K. Takada, K. Fukuda, N. Iyi, Y. Bando, T. Sasaki, Angew. Chem. Int. Ed. 46 (2007) 1.
[12] S.R. Ovshinsky, M.A. Fetcenko, J. Ross, Science 260 (1993) 176.
[13] W.K. Hua, M.M. Geng, X.P. Gao, T. Burchardt, Z.X. Gong, D. Noréus, N.K. Nakstad, J. Power Sources 159 (2006) 1478.
[14] Q.D. Wu, X.P. Gao, G.R. Li, G.L. Pan, T.Y. Yan, H.Y. Zhu, J. Phys. Chem. C 111 (2007) 17082.
[15] R. Ferrando, J. Jellinek, R.L. Johnston, Chem. Rev. 108 (2008) 845.
[16] J.B. Sambur, B.A. Parkinson, J. Am. Chem. Soc. 132 (2010) 2130.
[17] Y.H. Deng, C.H. Deng, D.W. Qi, C. Liu, J. Liu, X.M. Zhang, D.Y. Zhao, Adv. Mater. 21 (2009) 1.
[18] Y-.K. Sun, S.-T. Myung, B.-C. Park, K. Amine, Chem. Mater. 18 (2006) 5159.
[19] Z.R. Chang, H.W. Tang, J.G. Chen, Electrochem. Commun. 1 (1999) 513.
[20] R.S. Jayashree, P.V. Kamath, J. Electrochem. Soc. 149 (2002) A761.

[21] F. Lichtenberg, K. Kleinsorgen, J. Power Sources 62 (1996) 207.
[22] W.K. Hu, X.P. Gao, M.M. Geng, Z.X. Gong, D. Noréus, J. Phys. Chem. B 109 (2005) 5392.
[23] Jpn. Patent No. 59 165 371 [84165370].
[24] D.H. Son, S.M. Hughes, Y.D. Yin, A.P. Alivisatos, Science 306 (2004) 1009.
[25] R.D. Robinson, B. Sadtler, D.O. Demchenko, C.K. Erdonmez, L.W. Wang, A.P. Alivisatos, Science 317 (2007) 355.
[26] C.Y. Xu, L. Zhen, R. Yang, Z.L. Wang, J. Am. Chem. Soc. 129 (2007) 15444.
[27] Q.H. Yao, I.U. Arachchige, S.L. Brock, J. Am. Chem. Soc. 131 (2009) 2800.
[28] J.M. Luther, H.M. Zheng, B. Sadtler, A.P. Alivisatos, J. Am. Chem. Soc. 131 (2009) 16851.
[29] B. Zhang, Y. Jung, H.-S. Chung, L.V. Vugt, R. Agarwal, Nano Lett. 10 (2010) 149.
[30] International Centre for Diffraction Data, Newton Square, PA, USA.
[31] I.G. Casella, M.R. Guascito, J. Electroanal. Chem. 476 (1999) 54.
[32] R. Barnard, C.F. Randell, F.L. Tye, J. Appl. Electrochem. 10 (1980) 109.
[33] D.A. Corringan, S.L. Knight, J. Electrochem. Soc. 136 (1989) 613.
[34] C. Faure, C. Delmas, M. Fouassier, J. Power Sources 35 (1991) 279.